

Mechanically Exfoliated Graphite for Highly Reversible Na-Storage with Carbon Coated $\text{Na}_3\text{V}_2(\text{PO}_4)_3$ Cathode with Low-Temperature Conditions

Shaji Jyothilakshmi, Yun-Sung Lee,* and Vanchiappan Aravindan*

Tremendous efforts are put forward to develop novel high-performance electrodes for Na-ion batteries (SIBs) in order to replace commercial Li-ion batteries (LIBs). Graphite, the most versatile anode for LIBs, fails to accommodate Na^+ ions owing to the poor thermodynamic stability of the binary graphite intercalation compound. This study aims to exfoliate the layers of graphite through a simple mechanical process at different time intervals (1, 5, 10, 20, 40, and 80 h) and examine the potential candidate for Na-storage in the presence of carbonate-based electrolytes. This study reports that ball milling plays a vital role in the performance of the graphite in Na-storage. The graphite exfoliated for 80 h (EG-80h) rendered an excellent reversible capacity of 209 mAh g^{-1} with coulombic efficiency of $>99\%$ after 100 cycles in EC-based electrolyte. In situ impedance analysis is performed to validate the charge storage mechanism and Na-ion kinetics. The performance of EG-80h in a full-cell assembly is evaluated with a carbon-coated $\text{Na}_3\text{V}_2(\text{PO}_4)_3$ cathode, which exhibited an initial capacity of $\approx 75 \text{ mAh g}^{-1}$ and energy density of 201 Wh kg^{-1} . In addition, the adaptability of the NVPC/EG-80h cell at different temperatures is examined from -10 to 50°C , displaying excellent performance in both high and low-temperature conditions.

the scarcity of lithium metal is increasing; meanwhile, only an insignificant amount of lithium is getting recycled.^[1] Therefore, there is an urgent need to develop some alternatives for lithium. Thanks to several years of research, the researchers found the ideal alternative, sodium. Due to the abundance of sodium in the earth's crust and oceans, reduced production cost, and improved safety, sodium-ion batteries (SIBs) have gained popular attention and interest.^[2] However, the extensive commercial application of SIBs has not made essential progress because of the inferior energy density and lack of suitable anode materials.^[3–5] Graphite has been the most promising and well established anode in commercial LIBs, but inferior thermodynamic stability of Na-based binary graphite intercalation compound (*b*-GIC) is a main setback of SIBs. Since the utilization of ether-based electrolytes, the formed $[\text{Na-co-solvent}]^+$ can easily intercalate into the graphitic layers to form a stable ternary graphite intercalation compound (*t*-GIC).^[6,7]

1. Introduction

The demand for renewable energy sources is increasing as conventional energy produces fossil fuels, which will get depleted within a few decades. However, most renewable energy sources are intermittent and discontinuous, resulting in the necessity of developing energy storage devices. Batteries are the most preferred choice, among them, lithium-ion batteries (LIBs) flourished and become the game changer in battery technologies. However, when considering the fact that upon the increasing demand for LIBs in electric vehicles and extensive grid services,

The reversible de/insertion of Na-ions into the graphite using carbonate-based electrolytes remains an unattainable goal due to the formation of an unstable *b*-GIC. Cao et al.^[8] theoretically predicted that Na^+ can be inserted into graphite with interlayer spacing not less than 0.37 nm . Similarly, amorphous carbon materials with more lattice defects and disordered structures can be chosen for reversible Na-storage.^[5,9,10] Amorphous carbon are two types: hard and soft carbons, which showed decent Na-storage properties due to more open structures, low degree of graphitization, disorder, and expanded layers.^[1,9] In 2010, Na-ions were successfully inserted into hard carbon, but the defect-rich disordered structure of hard carbon has low average sedation potential and poor electronic and ionic conductivities, resulting in below-par rate performance in batteries. On the contrary, soft carbon with a semi-graphitic structure with fewer defects and disorder is an ideal alternative to hard carbon. Soft carbon has greater crystallinity and electrical conductivity than hard carbon, resulting in improved rate performance of the battery. Regrettably, due to the narrow interlayer spacing in the graphitic domains, it was found difficult to intercalate relatively larger Na^+ ions.^{3,4,8,9}

S. Jyothilakshmi, V. Aravindan
Department of Chemistry
Indian Institute of Science Education and Research (IISER)
Tirupati 517619, India
E-mail: aravindan@iisertirupati.ac.in
Y.-S. Lee
School of Chemical Engineering
Chonnam National University
Gwang-ju 61186, Republic of Korea
E-mail: leey@chonnam.ac.kr

DOI: 10.1002/smll.202403935

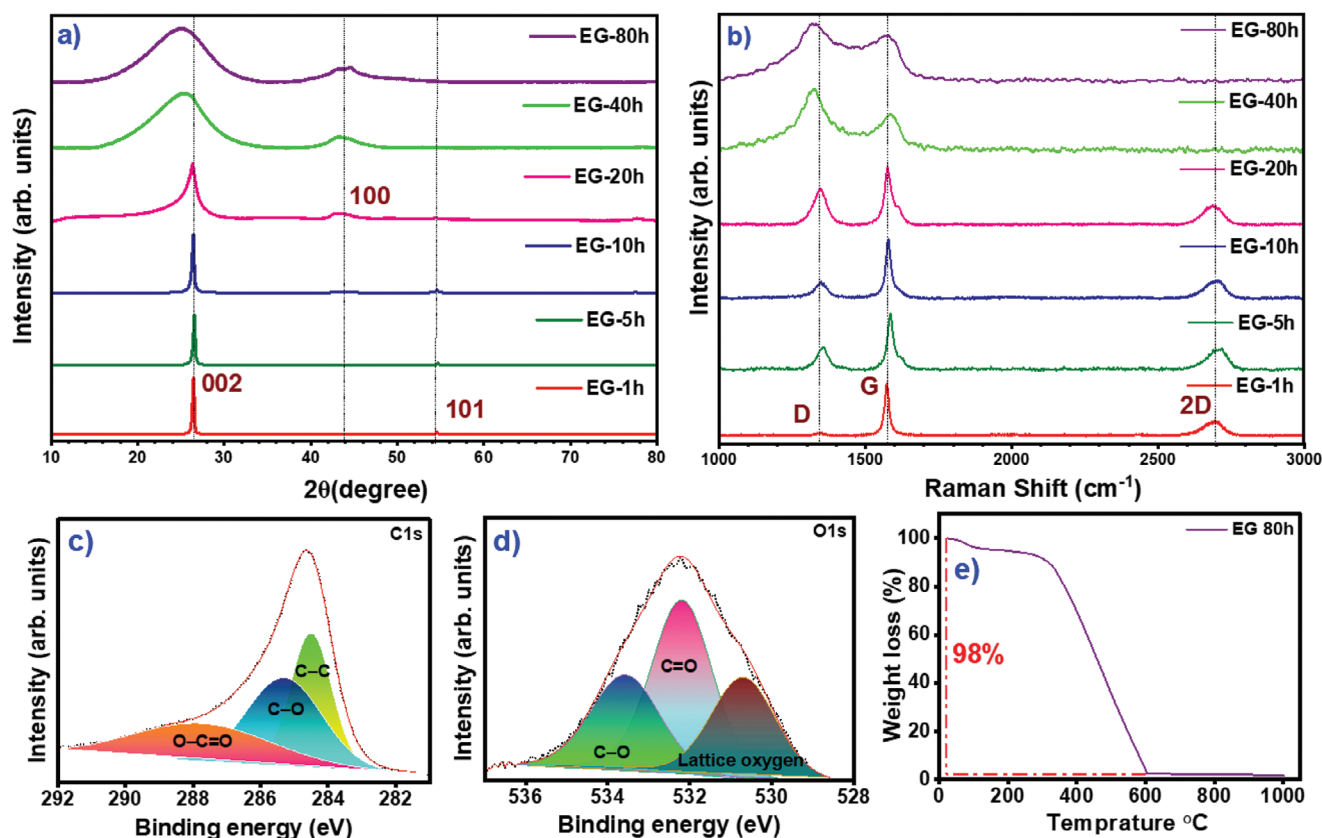


Figure 1. Physical characterization of EG: a) XRD pattern of EG samples corresponding to the ball milling time, b) Raman spectra of all the EG samples showing peaks corresponding to D, G, and 2D bands, deconvoluted XPS spectra of EG-80h showing the elements present c) C 1s and d) O 1s, and e) TGA spectra of EG-80h.

In this line, we aim to exfoliate the layers of graphite *via* simple mechanical methods and study the possibility of reversible Na-insertion using carbonate-based electrolyte. The novelty of this work is that we are the first to exfoliate the layers of graphite to study the sodium storage property. We report the successful exfoliation of the long-range order of the graphitic layer through ball milling at different time limits (1, 5, 10, 20, 40, and 80 h) to convert it into a short-range order. At the same time, the flaky morphology is well maintained. We report the electrochemical performance of exfoliated graphite (EG) in a half-cell assembly *vs.* Na, where EG-80h showed superior performance and was subsequently used for further studies. Further, we synthesized carbon-coated sodium superionic conductor (NASICON) type $\text{Na}_3\text{V}_2(\text{PO}_4)_3$ (NVPC) and paired it up with the EG-80h to fabricate a Na-ion full-cell and evaluated its performance. Also, a temperature-dependent study was carried out to analyze the feasibility of the NVPC/EG-80h assembly at different temperature conditions, which will be discussed in detail in the upcoming sections.

2. Results and Discussion

The physical structure of exfoliated graphite (EG) samples was examined through an X-ray diffraction (XRD) pattern, as shown in Figure 1a. The pattern of EG-1h shows a characteristic sharp peak $\approx 26^\circ$ corresponds to the (002) plane and matches well with

the XRD pattern of graphite (DB card no. 90 115 77) belonging to the space group $P6_3/mmc$. The sharpness of the peaks and absence of any other indicates the high crystallinity and purity of the EG-1h. As we compare the pattern of EG-1h with EG-5h, 10h, 20h, 40h, and 80h, we can see a shift in the peak at 26° to a lower 2θ value, indicating the reduction in particle size. The sharpness of the peaks is destroyed, and broader peaks are observed especially for EG-40h and 80h, indicating that the crystallinity of the graphite is destroyed to a certain extent. As the ball milling time increases, the graphitic layers get more exfoliated, where the long-range order of the graphite is converted to short-range order and becomes more amorphous in structure. The unit cell parameters are $a = b = 2.464 \text{ \AA}$, $c = 6.711 \text{ \AA}$, $\alpha = \beta = 90^\circ$, and $\gamma = 120^\circ$ with unit cell volume = 35.286 \AA^3 . The particle size of all the EG was calculated using the Debye–Scherrer equation:

$$D = K \lambda / \beta \cos \theta \quad (1)$$

where K is the constant (0.9), λ is the wavelength of the X-ray source used, β is the full width at half maximum of the peak in radians, and θ is the Bragg's angle in radians. The particle size was calculated to be $\approx 27, 24, 22, 3, 2$, and 1 nm for EG-1, 5, 10, 20, 40, and 80h, respectively. The XRD pattern and the Rietveld refined pattern of NVPC are shown in Figure S1a,b (Supporting Information), where all the peaks are very sharp and prominent reflections, indicating high purity and crystallinity.

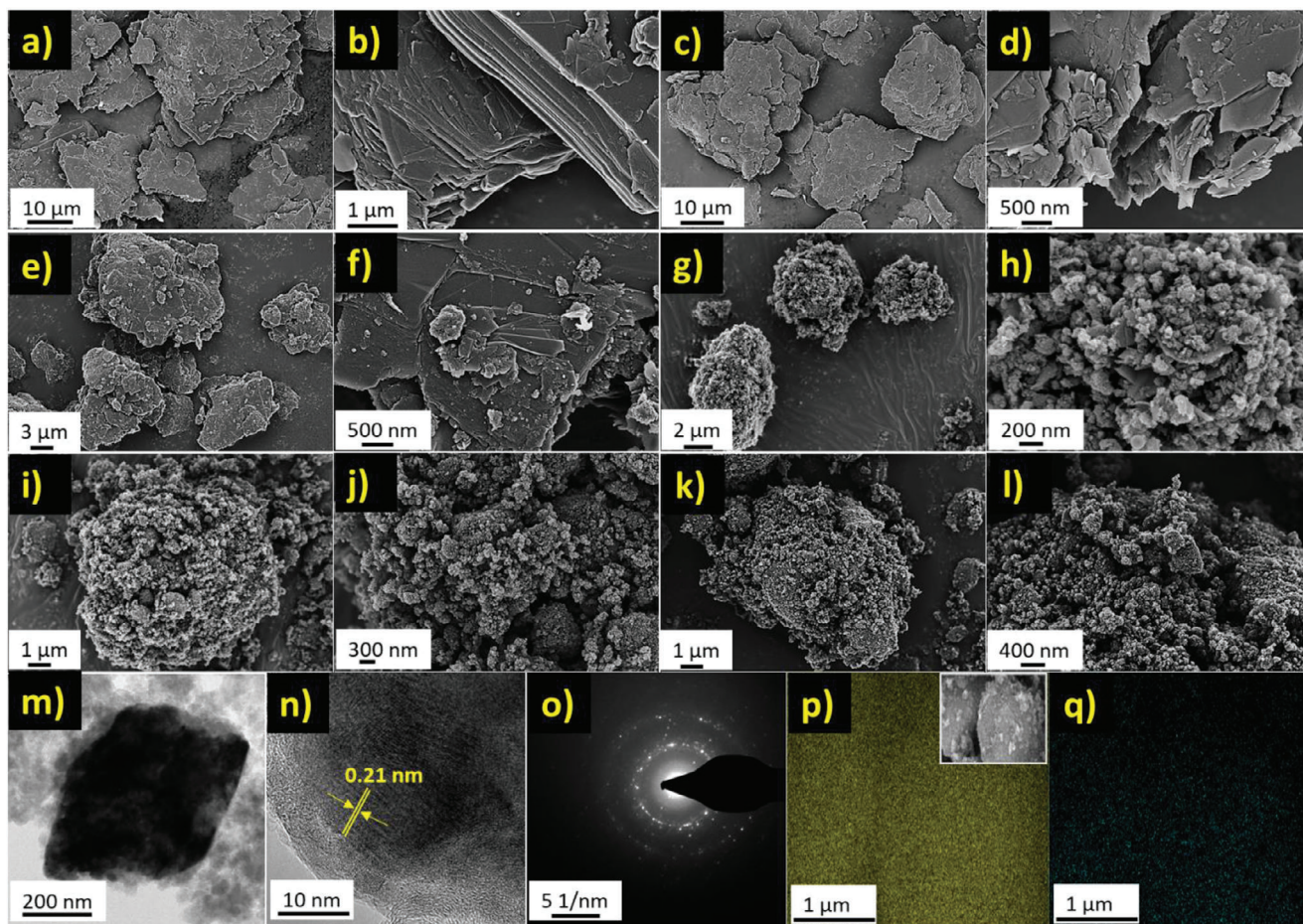


Figure 2. SEM images with different magnifications: a,b) EG-1h, c,d) EG-5h, e,f) EG-10h, g,h) EG-20h, i,j) EG-40h, and k,l) EG-80h, m,n) HR-TEM image of EG-80h, o) SEAD pattern of EG-80h, and p,q) elemental mapping of EG-80h showing the presence of C & O.

Figure 1b represents the Raman spectra of all the EG samples, showing peaks near 1572, 1341, and 2697 cm^{-1} corresponding to the D, G, and 2D bands, respectively, of the carbonaceous material.^[7] The absence of the D band in the EG-1h indicates the highly ordered crystalline structure. In Raman spectra of EG-5, 10, and 20h well, distinguished G, D, and 2D bands are observed, suggesting the presence of both disordered and ordered graphite.^[11] However, in the case of EG-40 and 80h, the intensity of the D band is higher than the G band, and the 2D band is absent, representing the absence of the graphitic sp^2 bond. The degree of disorder or graphitization can be calculated from the I_D/I_G ratio, which is ≈ 0.3 for EG-5h and 10h, 0.6 for EG-20h, and >1.2 in the case of EG-40h and 80h. The value >1.2 indicates that the graphite becomes more amorphous and disordered in structure after exfoliation.^[12] The nitrogen adsorption-desorption isotherm, along with the pore size distribution curve for all EG samples, are shown in Figure S2 (Supporting Information). When we compare the BET surface area and BJH pore size distribution values (Table S1, Supporting Information), it is found that as the exfoliating time increases, the surface area and pore radius increase to the extent that any further exfoliation results in the decrease of surface area and pore radius. This may be due to the agglomeration of particles as the ball milling

time increases. Figure 1c,d shows the deconvoluted C 1s and O 1s X-ray photoelectron spectra (XPS) of EG-80h, confirming the presence of carbon and oxygen. The deconvoluted C1s peak split into three peaks with maximum binding energy at 284.5, 285, and ≈ 287.7 eV belonging to the C–C bond in graphite, C–O groups, and O=C–O groups, respectively.^[13,14] The O 1s spectra display three asymmetric peaks at binding energy values of ≈ 533.6 , ≈ 532 , and ≈ 530 eV, corresponding to oxygen in O–C bonds, oxygen in O=C bonds, and oxygen components adsorbed on the surface of the material, respectively.^[15,16] The carbon content in EG-80h is estimated through thermogravimetric analysis (TGA) (Figure 1e). TGA was performed from room temperature to 1000 $^{\circ}\text{C}$ at a scan rate of 10 $^{\circ}\text{C min}^{-1}$ in an air atmosphere. There was no significant weight loss till 300 $^{\circ}\text{C}$, after this, a sharp decrease in the sample weight of 98% is observed, which corresponds to the decomposition of the carbonaceous materials.

Figure 2 displays the scanning electron microscope (SEM) images of all EG samples at different magnifications. From the SEM images of EG-1h, the flaky nature and the layers of graphite are very prominent (Figure 2a,b). However, as the ball milling time increases, we can observe that the layers are getting destroyed, and the particle size is getting decreased and more agglomerated (Figure 2c–l). This indicates that the long-range order of graphite

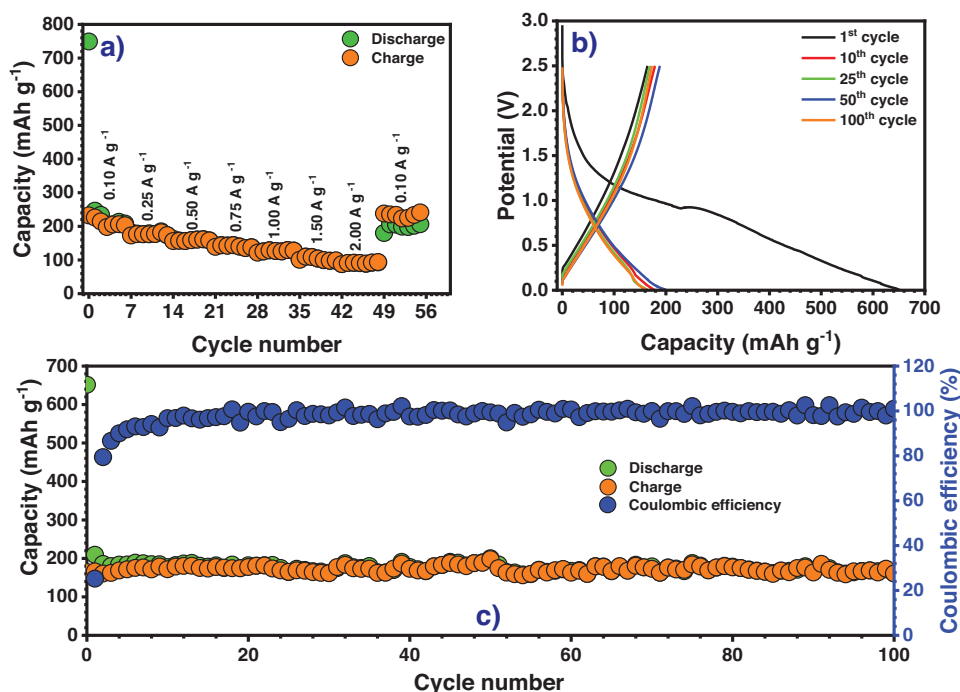


Figure 3. Electrochemical characterization of Na/EG-80h cell in EC-based electrolyte: a) rate performance at different current rates, b) charge–discharge curves at 1st, 10th, 25th, 50th, and 100th cycles, c) cycling stability performance at a current density of 0.1 A g⁻¹.

is converted into a short-range ordered one; nevertheless, the flaky nature is maintained. The high-resolution transmission electron microscope (HR-TEM) images (Figure 2m) reveal the flaky agglomerated morphology of EG-80h. Figure 2n represents the lattice fringes of EG-80h obtained through HR-TEM with a lattice fringe width of 0.21 nm. The selected area electron diffraction (SAED) pattern (Figure 2o) shows small bright spots in concentric rings, indicating the polycrystallinity of the sample. The elemental mapping of EG-80h is shown in Figure 2p,q, which further confirms the presence of carbon and oxygen elements on the surface of the material. As far as the counter electrode is concerned, the SEM images of NVPC at two different magnifications are shown in Figure S3 (Supporting Information), which represents the porous structure of the synthesized NASICON phase.

2.1. Electrochemical Studies

2.1.1. Half-Cell Performance

The electrochemical performance of EG was analyzed through a Na/EG assembly. Initially, we tried to study the performance of all the samples of EG with two types of carbonate-based electrolyte. Figure S4 (Supporting Information) represents galvanostatic charge–discharge curves of commercial graphite (CG) without ball milling and EG at different ball milling durations in 1 M NaClO₄ in EC: DMC: 5%FEC electrolyte. The results clearly state that ball milling plays a vital role in the performance of the cell. As the duration of ball milling increases, the exfoliation of graphitic layers results in the fast de/insertion of Na-ions with an enhanced capacity of EG. Among all the EGs, the graphite exfoliated for

80h (EG-80h) exhibited the maximum capacity; therefore, this EG-80h was used for further electrochemical studies. We have also evaluated the performance of EG-80h in the glyme-based electrolytes (Figure S5, Supporting Information) and observed that the initial capacity is higher when comparing the carbonate-based electrolyte, irrespective of the EC and PC-based solutions. However, the rate performance at the higher current rate is very poor, and the cell could not withstand its stability throughout cycling in both low and high current rates in glyme solutions compared to esters. The cyclic voltammetry (CV) traces of the Na/EG-80h cell were performed from 0.005 to 2.5 V vs. Na at a scan rate of 0.1 mV s⁻¹ for the first two cycles, as shown in Figure S6 (Supporting Information). A very prominent peak at 0.8 V vs. Na in the first cycle represents the decomposition of the electrolyte solution and subsequent formation of the solid electrolyte interface (SEI), which causes huge irreversibility in the cell performance. In the cathodic scan, the broad peak at ≈0.01 V vs. Na and a similar peak at ≈0.3 V vs. Na on the anodic side represents Na-storage in the EG-80h. The performance of EG-80h with an increase in current rates was studied in both the EC and PC-based electrolytes, which displayed promising results, as shown in Figures 3a and S7a (Supporting Information). The cell displayed a capacity of 90 mA g⁻¹ at a higher current rate of 2 A g⁻¹. After cycling at a higher current rate, when the cells were switched to a low current, the cells were able to retain the initial capacity, indicating the robustness and structural stability of the material in EC and PC-based solutions. The Galvanostatic charge–discharge (GCD) curves at the 1st, 10th, 25th, 50th, and 100th cycles are shown in Figures 3b and S7b (Supporting Information). It is seen that the reversibility of Na-ions in half-cells with EC electrolytes was much higher and more stable

than that of PC electrolytes. The curves are more sloping than plateaus, reflecting the broad peaks in CV. This indicates that Na⁺-ions are first intercalated into the EG-80h matrix and then followed by absorption.^[17,18] The long-term cycling profile of EG-80h in EC and PC over 100 cycles at a current rate of 0.1 A g⁻¹ is shown in Figures 3c and S7c (Supporting Information), respectively. The Na/EG-80h cell with EC-based electrolyte exhibited superior performance and stability with an initial reversible capacity of 209 mAh g⁻¹ (PC electrolyte-176 mAh g⁻¹) and a coulombic efficiency of >99% after 100 cycles. From the results, we concluded that Na/EG-80h cells displayed promising results in EC-based electrolytes.

The in situ electrochemical impedance spectroscopy (in situ EIS) study was performed to understand the Na-storage of Na/EG-80h cell. Figure 4 illustrates the detailed Nyquist plot of the changes in each potential during charge–discharge for the 1st, 5th, 10th, and 25th cycles. We observed a very high R_{CT} value during discharge in the first cycle, which decreased in the following cycles, indicating the formation of a SEI layer in the first cycle. In the initial cycles, the charge storage is mainly contributed by faradaic reactions, but after 5th cycle, there is no prominent change in the R_{CT}, and we could see the diminishing of the semicircle, which implies that the charge storage involves both faradaic and non-faradaic mechanisms supporting the results obtained from CV and GCD studies. From the 5th cycle, we could see consistency throughout the charge–discharge, ensuring the stability and ability of the cell to withstand large numbers of cycling without any failure.

Parallely, we have synthesized a carbon-coated sodium superionic conductor (NASICON) type Na₃V₂(PO₄)₃ (NVPC) and studied its electrochemical performance with the same EC-based electrolyte combination in Na/NVPC half-cell configuration. Figure S8a (Supporting Information) shows the CV curves of NVPC at different scan rates of 0.1, 0.2, 0.4, 0.6, 0.8, and 1 mV s⁻¹ tested between a potential window of 2.5 to 3.8 V vs. Na. During the anodic and cathodic scan at 0.1 mV s⁻¹, we can see prominent peaks positioned approximately at 3.4 and 3.3 V vs. Na, respectively, which corresponds to V³⁺ to V⁴⁺ and V⁴⁺ to V³⁺ redox transitions.^[6,19,20] This pair of redox peaks represents two Na⁺ ions insertions into/extractions from the host Na₃V₂(PO₄)₃, and the intermediate phase is NaV₂(PO₄)₃.^[7,19,21,22] Figure S8b (Supporting Information) represents the galvanostatic rate performance of NVPC from lower to higher current rates of 0.05, 0.1, 0.25, and 0.5 A g⁻¹. The NVPC could sustain high current application, displaying excellent structural stability. The GCD pattern for rate performance of NVPC at different current rates (Figure S8c, Supporting Information) shows a plateau ≈3.4 V vs. Na, confirming that Na⁺ storage occurs through the oxidation-reduction of the V³⁺/V⁴⁺ couple.^[12,23,24] The charge–discharge curve for the 1st, 25th, 50th, and 100th cycle is represented in Figure S8d (Supporting Information), indicating good cycling stability of the NVPC with a capacity retention of >95% after 100 cycles. The long-term cycling stability of NVPC at a current density of 0.05 A g⁻¹ between a potential window of 2.5 to 3.8 V vs. Na is shown in Figure S8e (Supporting Information). The Na/NVPC cell exhibited an initial reversible capacity of 110 mAh g⁻¹ with a coulombic efficiency of 99% over 100 cycles.

2.1.2. Full-Cell Performance

The full cell was fabricated with EG-80h as the anode, NVPC as the cathode, and EC as the electrolyte and was tested in a potential window of 1.2 to 3.6 V. The EG-80h electrodes were pre-cycled three times before assembling into a balanced full cell with an NVPC electrode to mitigate the irreversibility of EG-80h and ensure the half-cell results as well. The mass of the NVPC cathode material was balanced with the capacity of the EG-80h anode material. The anodic and cathodic scan at a low scan rate of 0.1 mV s⁻¹ shows a broad peak ≈3V (Figure 5a), which gets shifted to a lower potential region as the scan rate increases, corresponding to the capacity contribution. The rate performance of NVPC/EG-80h cell at different current densities is shown in Figure 5b, which represents that the cell can withstand high current and revert back to the initial capacity at low current rates. This confirms that the electrodes are compatible with high-current applications without any structural damage that can cause the sodium storage ability of the material. It is well established that the carbonaceous anode involves multi-phase storage mechanisms like pore filling, adsorption, chemisorption at defective sites, and interaction of Na-ions with nanopores and metal cluster formation. When the cell is tested at lower scan rates, the carbonaceous anodes require a few cycles to form a stable solid electrolyte interphase (SEI), and the Na-adsorption/desorption process is limited. When cycling progresses, the polarization tends to increase due to the robust nature of the SEI layer, and the increase in the adsorption/desorption process eventually results in a reduction in the net cell potential. In the CV profile, a fresh full-cell is fabricated and tested at three cycles in each scan rate. Concurrently, exactly the same trend is observed in the galvanostatic performance (Figure 5c). At the initial cycle, the cell potential is found to be higher (≈3.15 V), which slowly drops (≈2.75 V at the 100th cycle) during the extended cycling. Poor SEI formation over the carbonaceous anode is the main culprit for the deviation in the cell potential. Parallely, the deviation in the potential is validated in terms of change in the R_{CT} values from the in situ impedance as well. Figure 5c,e displays the cycling stability profile of NVPC/EG-80h cell at a current rate of 0.15 A g⁻¹ and charge–discharge curves at 1st, 25th, 50th, and 100th cycles, respectively. The cell exhibited promising performance with an initial discharge capacity of 71 mAh g⁻¹ and a coulombic efficiency of 97% over 100 cycles.

Additionally, the adaptability of the full cell at different temperature conditions was studied. The full cell was cycled for 200 cycles at different temperatures at 1 A g⁻¹ current density, as shown in Figure 6. We cycled the cell at temperatures of –10, 0, 10, 25, and 50 °C, and it displayed >99, 98, 98, 95, and 82% capacity retention, respectively. The cell rendered excellent performance in both low and high temperatures, ensuring the stability and applicability of the material to operate at high and sub-zero temperatures without any cell failure. A Ragone plot was constructed with energy density and corresponding power density values at different current densities and temperatures, as represented in Figure 5d. The cell displayed a very promising energy density and power density of 201 Wh kg⁻¹ and 4.5 kW kg⁻¹, respectively, calculated based on the total mass of the anode and cathode active material. Considering all the above-discussed results, we can

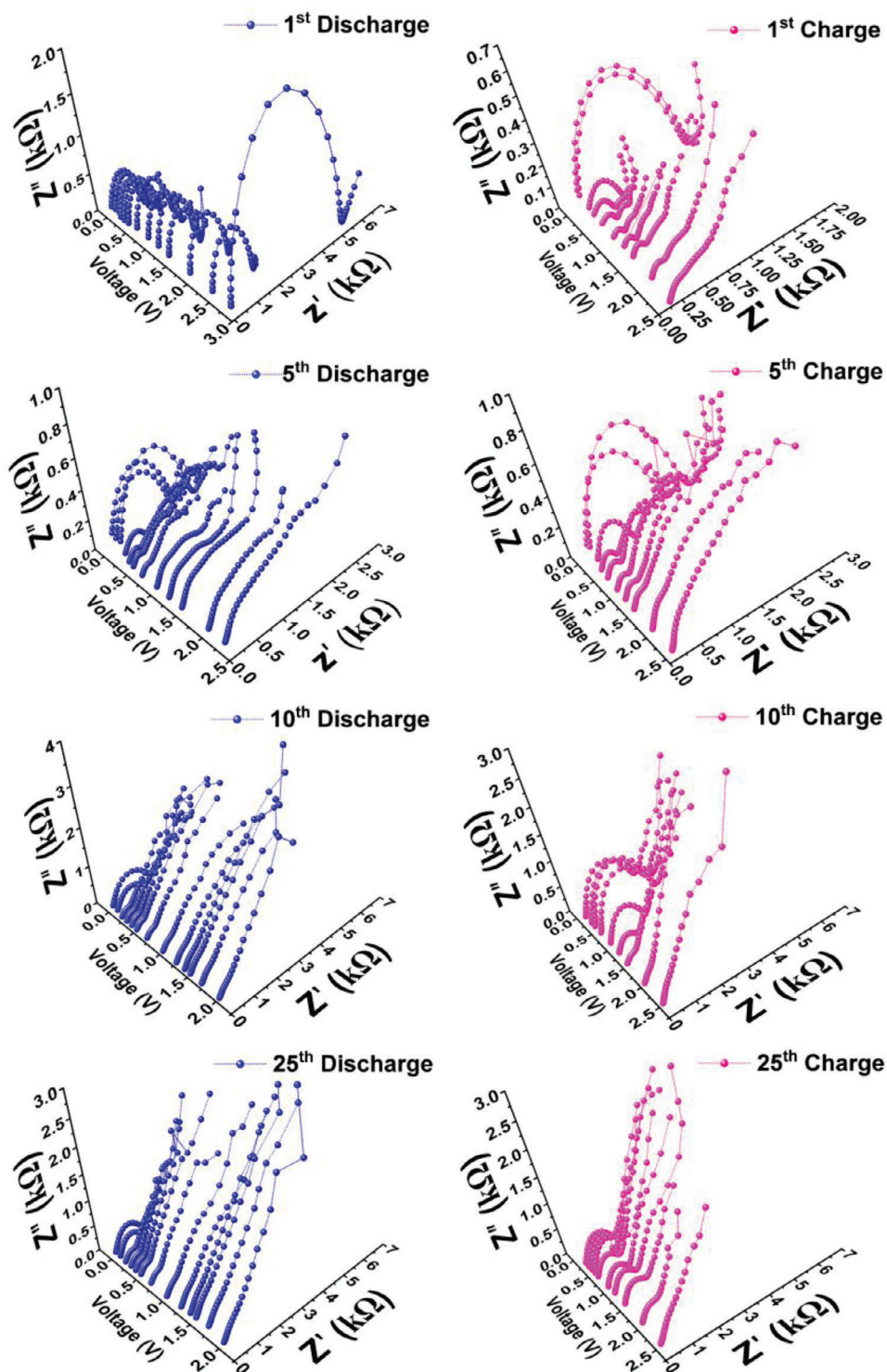


Figure 4. In situ EIS for the 1st, 5th, 10th, and 25th cycles at fixed potentials.

conclude that graphite exfoliation opens up a new avenue toward sodium storage application with a very high energy and power density. On the other hand, more in-depth studies are required to understand the exact charge-storage mechanism of graphitic carbons.

3. Conclusion

We have exfoliated the graphitic layer via a simple mechanical process by ball milling the graphite at different time intervals (1, 5, 10, 20, 40, and 80h), where we tried to break the long-range

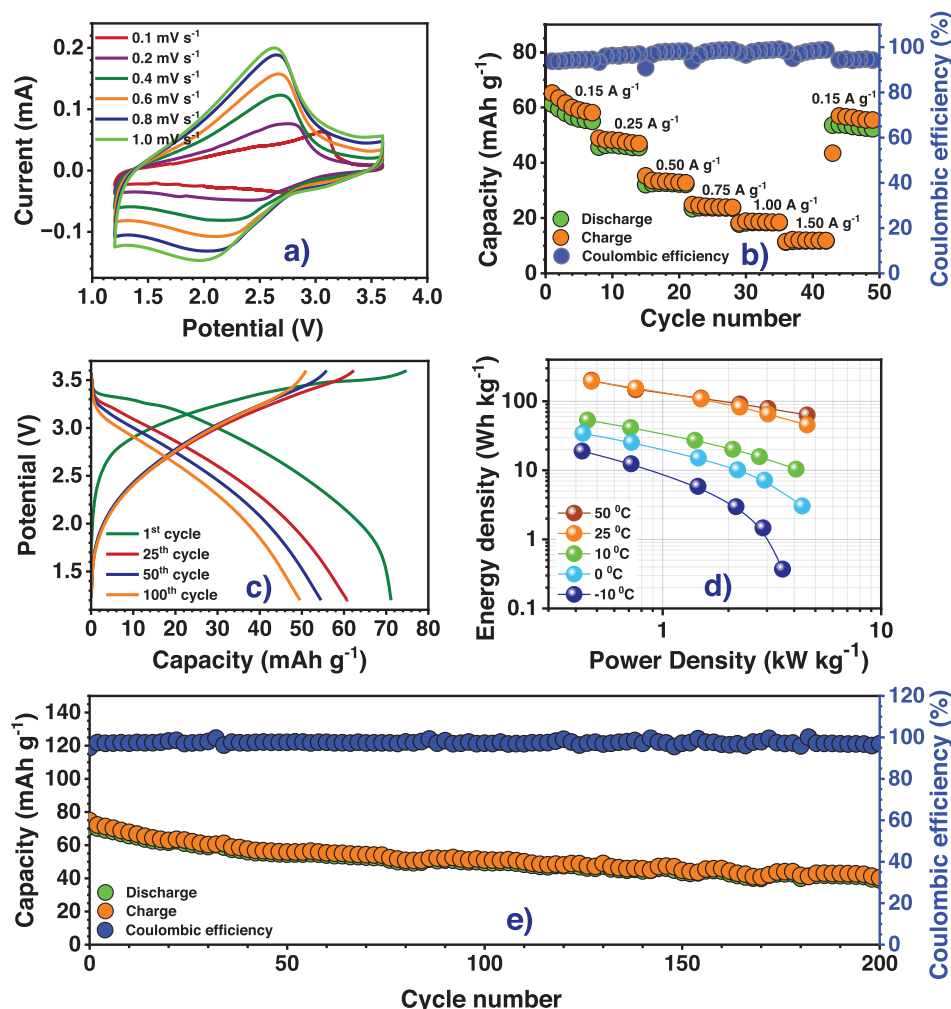


Figure 5. NVPC/EG-80h full-cell performance in EC-based electrolyte: a) cyclic voltammetry curves, b) rate performance with coulombic efficiency, c) charge–discharge curves at 1st, 25th, 50th, and 100th cycles, d) Ragone plot based on the total active material mass of anode and cathode and e) cycling profile with coulombic efficiency at a current density of 0.15 A g^{−1} between 1.2 and 3.6 V.

order of graphite and study the possibility of Na-ion insertion process. The electrochemical performance of the exfoliated graphite (EG) for sodium-ion storage was analyzed using carbonate-based electrolytes (1 M NaClO₄ in EC: DMC:5%FEC, (EC)& 1 M NaClO₄ in PC: DMC:5%FEC, (PC)). It is observed that there is a remarkable increase in the capacity of the graphite as the exfoliation time increases. The preliminary experiments showed that graphite ball milled for 80h (EG-80h) exhibited promising results in the EC electrolytes system in terms of reversible capacity (209 mAh g^{−1}), stability, rate performance, and coulombic efficiency (99% after 100 cycles). We have also synthesized carbon-coated sodium superionic conductor (NASICON) type Na₃V₂(PO₄)₃ (NVPC) and analyzed the electrochemical performance in the same carbonate-based electrolyte combination. Then, we fabricated a Na-ion battery (SIB) by combining NVPC as the cathode and EG-80h as the anode and studied their sodium-ion storage application. The assembled battery exhibited a very high energy density of 201 Wh kg^{−1} and a power density of 4.5 kW kg^{−1}. Also, we have examined the feasibility of the battery at different temperature conditions (−10, 0, 10, 25, and 50 °C) and

observed that the SIB rendered a very stable performance at both low and high temperatures. This study opens up a new avenue toward the Na-ion storage in graphite with esters.

4. Experimental Section

Exfoliation of Graphite: The commercial graphite was exfoliated using a scalable mechanical process. The graphite was ball milled at 300 rpm in a Retsch PM 200 planetary ball miller with a 20:1 ball-to-material mass ratio at different time intervals (1, 5, 10, 20, 40, and 80 h). The graphite exfoliated at 1, 5, 10, 20, 40, and 80 h was represented as EG-1h, EG-5h, EG-10h, EG-20h, EG-40h, and EG-80h, respectively.

Synthesis of Carbon Coated Na₃V₂(PO₄)₃ (NVPC): The cathode NVPC has been synthesized via the sol-gel method.^[21] In the typical synthesis process, stoichiometric amounts of NaOH (Sigma–Aldrich, >98%), NH₄H₂PO₄ (Sigma–Aldrich, >98%), NH₄VO₃ (Sigma–Aldrich, >99%) were dissolved in a minimum quantity of deionized (DI) water in a molar ratio of 3:3:2. To this mixture citric acid (Sigma–Aldrich, >99.5%) dissolved in DI water was added dropwise under violent stirring at 80 °C until it forms a dark blue gel. The color change from yellow to green to blue was clearly seen, an indication of electron transfer from V²⁺ to V³⁺ to V⁴⁺.

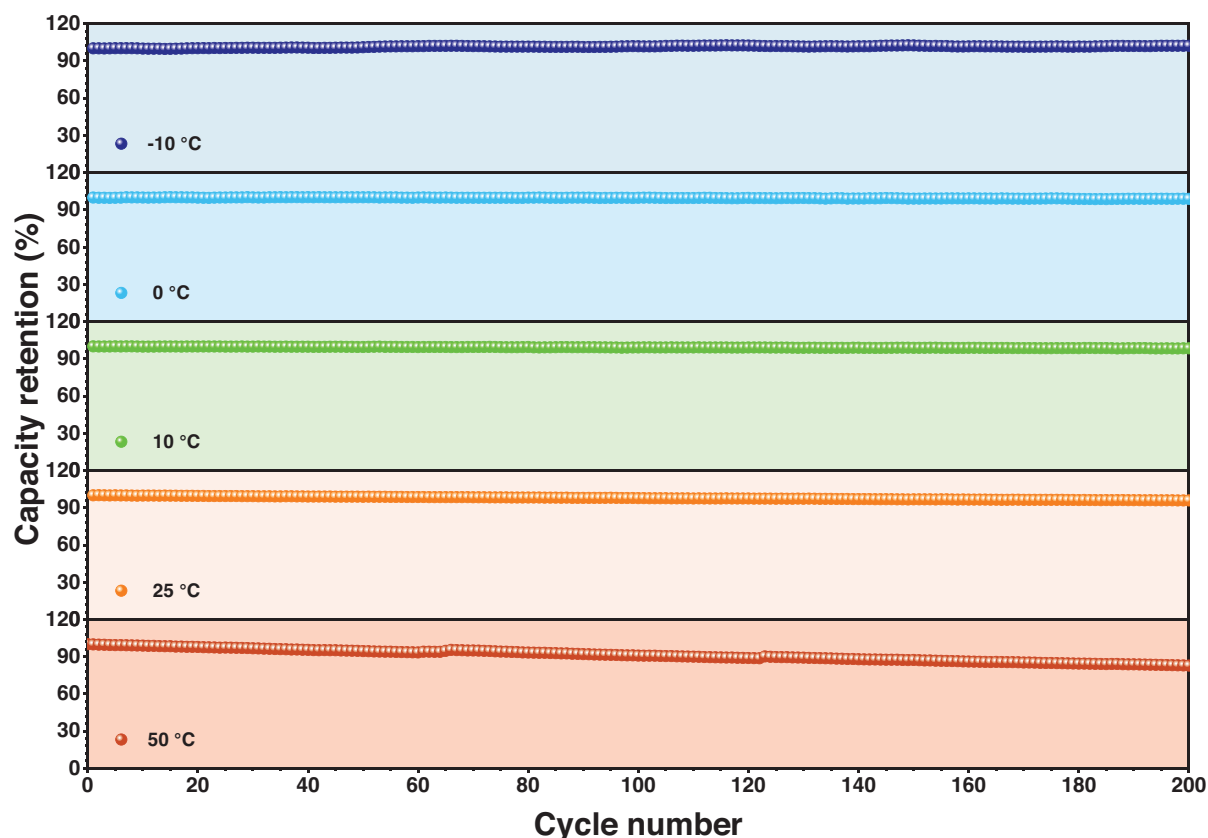


Figure 6. Cycling profile of the same NVPC/EG-80h full-cell at a current density of 1 A g^{-1} for 200 cycles between 1.2 and 3.6 V at temperatures of -10 , 0 , 10 , 25 , and 50 °C.

Then, the gel was dried in an oven at 80 °C for 12 h in an air atmosphere, followed by grounding and calcination at 350 °C for 3 h under argon flow in a tube furnace. After natural cooling, the powder was heated at 800 °C for 16 h in an argon atmosphere to obtain NVPC.

Material Characterization: Structural characterization of exfoliated graphite (EG) and $\text{Na}_2\text{V}_3(\text{PO}_4)_3$ (NVPC) were performed in Rigaku Smartlab automated multipurpose X-ray diffractometer with a monochromatic Cu K α radiation ($\lambda = 1.5604$ Å) at a scan rate of 1 min^{-1} . Raman spectroscopy was used to analyze the material composition of the samples in a Raman HR800 UV Raman microscope (Horiba Jobin–Yvon, France) with a 515 nm diode laser as a light source at room temperature. The surface elemental chemistry of the materials was studied using X-ray photoelectron spectroscopy (XPS, Multilab, 2000, UK). The surface morphology of the material was studied through field emission scanning electron microscopy (FE-SEM, Zeiss Gemini 560, Germany) and high-resolution transmission electron microscopy (HR-TEM, JEM-2000, EX-II, JEOL, Japan) to obtain high-resolution crystal structure. The physical properties of EG were determined through BET measurements (automated gas sorption analyzer, Autosorb IQ-XR-XR, 3 stat, Viton). The thermal decomposition of the EG was done using thermogravimetric analysis (TGA, Shimadzu, Japan), with a ramp rate of 5 °C min^{-1} in the air atmosphere.

Electrochemical Characterization—Electrode Fabrication—EG Electrode: The EG electrodes were fabricated by a slurry coating technique where EG was coated on Cu-foil with the conductive additive acetylene black (AB) and polyvinylidene fluoride (PVDF) as the binder in a ratio of 60:30:10 wt.% (EG:AB:PVDF). First, the PVDF was dissolved in 1-methyl-2-pyrrolidinone (NMP, anhydrous, 99.5%, Sigma–Aldrich), then AB and EG were mixed thoroughly using mortar and pestle and added to the PVDF-NMP solution to form a slurry. Then, the slurry was kept overnight, stirring at room

temperature to ensure homogeneity, and cast onto a copper foil with the help of a Doctor blade apparatus. This Cu-foil was kept for drying at 65 °C until NMP evaporates completely. After drying, it was pressed using a calendar roller machine and cut into 12 mm diameter electrodes using an electrode cutter.

Electrochemical Characterization—Electrode Fabrication—NVPC Electrode: NVPC free-standing electrode film for the Na-ion battery was hand-made using mortar and pestle. Active material (NVPC), acetylene black (AB), and teflonized acetylene black (TAB-2, binder) were taken and mixed in a ratio of 10:2:2 using ethanol as the solvent. A thin electrode film of NVPC was made and pressed onto a 14 mm stainless steel mesh (SS, Goodfellow, UK) current collector using a hydraulic press (Specac, UK). For full-cell fabrication, NVPC electrodes were made by adjusting the mass to balance the capacity of the anode during precycling.

Electrochemical Characterization—Electrolyte Preparation: The electrolytes were prepared inside the argon-filled glove box by dissolving NaClO_4 salt (Sigma–Aldrich, 98%) in various solvents such as ethylene carbonate (EC, Sigma, anhydrous, 99%), propylene carbonate (PC, Sigma, anhydrous, 99.7%), dimethyl carbonate (DMC, Sigma, anhydrous, >99%), in 1:1 ratio and 5% of additive fluoroethylene carbonate (FEC, Sigma, anhydrous, >99%). The salts and the solvents were directly used without any further purification. The electrolytes 1 M NaClO_4 in EC:DMC:5% FEC and 1 M NaClO_4 in PC:DMC:5%FEC were represented as EC and PC, respectively.

Electrochemical Characterization—Half-cell and Full-cell Fabrication: Before cell fabrication, the EG electrodes were kept in a vacuum oven for at least 4 h at 75 °C, whereas NVPC was kept for a minimum of 24 h to ensure the complete removal of moisture from the surface of the electrode. In the half-cell fabrication of both EG and NVPC, sodium metal was

used as the reference and counter electrode. Both half and full-cells have been assembled in an argon-filled glove box workstation (MBraun, Germany, $O_2 < 0.1$ ppm and $H_2O < 0.1$ ppm) in a CR2016 coin cell using a glass microfiber separator (Whatmann, cat no. 1825-047, UK). For full-cell fabrication, EG was pre-sodiated for three cycles and taken into the glove-box to decrimp it to assemble the full-cell with previously made mass-balanced NVPC electrode. The anode areal mass loading of active material for the full-cell was $\approx 3 \text{ mg cm}^{-2}$. BioLogic battery tester (BCS-805) was used to study the electrochemical performance of the assembled half-cell and full-cell, and an Espec SU-242 benchtop-type environmental chamber was used to perform temperature-dependent studies of the cells.

Supporting Information

Supporting Information is available from the Wiley Online Library or from the author.

Acknowledgements

The authors thank Mr. Nikhil Subash for the Rietveld refinement pattern of XRD. S.J. thanks the Prime Minister's Research Fellowship (0902009) for financial support. Y.-S.L. acknowledges the financial support from the National Research Foundation of Korea (NRF) grant funded by the Korean government (Ministry of Science, ICT&Future Planning) (No. RS-2023-00208361). V.A. acknowledges financial support from the Anusandhan National Research Foundation (ANRF), Govt. of India, through Swarnajayanti Fellowship (SB/SJF/2020-21/12) and Core Research Grant (CRG/2023/000013).

Conflict of Interest

The authors declare no conflict of interest.

Data Availability Statement

The data that support the findings of this study are available from the corresponding author upon reasonable request.

Keywords

anode, exfoliation, full-cell, graphite, $Na_3V_2(PO_4)_3$ cathode, Na-ion battery

Received: May 15, 2024

Revised: July 3, 2024

Published online:

- [1] S. Sarkar, S. Roy, Y. Hou, S. Sun, J. Zhang, Y. Zhao, *ChemSusChem* **2021**, *14*, 3693.
- [2] C. Nithya, S. Gopukumar, *WIREs Energy Environ.* **2015**, *4*, 253.
- [3] P. Thomas, D. Billaud, *Electrochim. Acta* **2001**, *46*, 3359.
- [4] H. Kang, Y. Liu, K. Cao, Y. Zhao, L. Jiao, Y. Wang, H. Yuan, *J. Mater. Chem. A* **2015**, *3*, 17899.
- [5] S. Komaba, W. Murata, T. Ishikawa, N. Yabuuchi, T. Ozeki, T. Nakayama, A. Ogata, K. Gotoh, K. Fujiwara, *Adv. Funct. Mater.* **2011**, *21*, 3859.
- [6] K. Subramanyan, M. Akshay, Y. S. Lee, V. Aravindan, *Adv. Mater. Technol.* **2022**, *7*, 2200399.
- [7] K. Subramanyan, Y. S. Lee, V. Aravindan, *J. Colloid Interface Sci.* **2023**, *632*, 326.
- [8] Y. Cao, L. Xiao, M. L. Sushko, W. Wang, B. Schwenzer, J. Xiao, Z. Nie, L. V. Saraf, Z. Yang, J. Liu, *Nano Lett.* **2012**, *12*, 3783.
- [9] H. Hou, X. Qiu, W. Wei, Y. Zhang, X. Ji, *Adv. Energy Mater.* **2017**, *7*, 1602898.
- [10] X. Dou, I. Hasa, D. Saurel, C. Vaalma, L. Wu, D. Buchholz, D. Bresser, S. Komaba, S. Passerini, *Mater. Today* **2019**, *23*, 87.
- [11] N. Díez, A. Iwak, S. Gryglewicz, B. Grzyb, G. Gryglewicz, *RSC Adv.* **2015**, *5*, 81831.
- [12] K. Subramanyan, Y. S. Lee, V. Aravindan, *J. Colloid Interface Sci.* **2021**, *582*, 51.
- [13] R. I. R. Blyth, H. Buqa, F. P. Netzer, M. G. Ramsey, J. O. Besenhard, P. Golob, M. Winter, *Appl. Surf. Sci.* **2000**, *167*, 99.
- [14] H. Hantsche, *Adv. Mater.* **1993**, *5*, 778.
- [15] Y. Xie, P. M. A. Sherwood, *Surf. Sci. Spectra* **1992**, *1*, 367.
- [16] S. Jyothilakshmi, P. Meshram, Abhilash, Y.-S. Lee, V. Aravindan, *Adv. Mater. Technol.* **2024**, *9*, 2301000.
- [17] D. A. Stevens, J. R. Dahn, *J. Electrochem. Soc.* **2001**, *148*, A803.
- [18] S. K. Saju, S. Chattopadhyay, J. Xu, S. Alhashim, A. Pramanik, P. M. Ajayan, *Cell Reports Phys. Sci.* **2024**, *5*, 101851.
- [19] W. Shen, C. Wang, H. Liu, W. Yang, *Chem. – A Eur. J.* **2013**, *19*, 14712.
- [20] F. Lalère, J. B. Leriche, M. Courty, S. Boulineau, V. Viallet, C. Masquelier, V. Seznec, *J. Power Sources* **2014**, *247*, 975.
- [21] S. Luo, J. Li, S. Bao, Y. Liu, Z. Wang, *J. Electrochem. Soc.* **2018**, *165*, A1460.
- [22] Y. Li, Y. Mei, R. Momen, B. Song, Y. Huang, X. Zhong, H. Ding, W. Deng, G. Zou, H. Hou, X. Ji, *Chem. Sci.* **2024**, *15*, 349.
- [23] Z. Deng, T. P. Mishra, E. Mahayoni, Q. Ma, A. J. K. Tieu, O. Guillon, J. N. Chotard, V. Seznec, A. K. Cheetham, C. Masquelier, G. S. Gautam, P. Canepa, *Nat. Commun.* **2022**, *13*, 4470.
- [24] B. Pandit, M. T. Sougrati, B. Fraisse, L. Monconduit, *Nano Energy* **2022**, *95*, 107010.